Planar-Dielectric-Wakefield Accelerator Structure Using Bragg-Reflector Boundaries

G. Andonian, O. Williams, S. Barber, D. Bruhwiler, P. Favier, M. Fedurin, K. Fitzmorris, A. Fukasawa, P. Hoang, K. Kusche, B. Naranjo, B. O'Shea, P. Stoltz, C. Swinson, A. Valloni, and J. B. Rosenzweig

Phys. Rev. Lett. **113**, 264801 — Published 30 December 2014

DOI: 10.1103/PhysRevLett.113.264801

Planar dielectric wakefield accelerator structure using Bragg-reflector boundaries

G. Andonian[1], O. Williams[1], S. Barber[1], D. Bruhwiler[2,5], P. Favier[1], M. Fedurin[3], K. Fitzmorris[1], A. Fukasawa[1], P. Hoang[1], K. Kusche[3], B. Naranjo[1], B. O'Shea[1], P. Stoltz[4], C. Swinson[3], A. Valloni[1], J.B. Rosenzweig[1*]

[1] *Department of Physics and Astronomy, UCLA, Los Angeles, California 90095, USA*

[2] *University of Colorado at Boulder, Center for Integrated Plasma Studies, Boulder, Colorado 80309, USA*

[3] *Accelerator Test Facility, Brookhaven National Laboratory, Upton, New York 11973, USA*

[4] *Tech-X Corporation, Boulder, Colorado 80303 USA and*

[5] *RadiaSoft LLC, Boulder, Colorado 80304, USA*

(Dated: October 29, 2014)

We report experimental measurements of narrowband, single-mode excitation, and drive beam energy modulation, in a dielectric wakefield accelerating structure with planar geometry and Bragg-reflector boundaries. A short, relativistic electron beam (∼1ps) with moderate charge (∼100pC) is used to drive the wakefields in the structure. The fundamental mode of the structure is reinforced by constructive interference in the alternating dielectric layers at the boundary, and is characterized by the spectral analysis of the emitted coherent Cherenkov radiation signal. Data analysis shows a narrowband peak at 210GHz corresponding to the fundamental mode of the structure. Simulations in both 2D and 3D provide insight into the propagating fields and reproduction of the electron beams dynamics observables and emitted radiation characteristics.

Electron-beam driven, dielectric wakefield acceleration (DWA) schemes initially demonstrated application as alternative acceleration techniques in scaled experiments in the 1980's [1]. Extension of these methods to reach sustained accelerating fields exceeding ≥GV/m is necessary to demonstrate viability of DWA as a future compact accelerator for high-energy collider schemes and high-brightness light source applications. Advances in nano- and micro-fabrication techniques and materials, and the introduction of high permittivity custom dielectrics, coupled with improved drive electron beam quality, has allowed experimental access to the ≥GV/m regime via terahertz-scale (THz, sub-mm wavelength) structures. The necessity to operate in the THz regime arises from two important considerations. In general, one cannot afford the stored electromagnetic energy at longer wavelengths (such as existing cm-wave linear accelerators) at such high fields; further, for the wakefield accelerator to reach GV/m, one should have small structure dimensions that yield efficient beam-structure coupling [2]. Recently, DWA experiments operating in the THz regime have yielded a myriad of experimental results, including: ≥5 GV/m field breakdown [2]; demonstration of narrowband THz generation and modal characterization [3]; selective resonant excitation using periodic drive beams [4]; and energy modulation in planar geometries [5, 6]. These results, while giving an experimental understanding of the DWA, have not until now addressed an important aspect of THz-regime accelerator structures − the use of metal boundaries to confine the electromagnetic modes in these structures introduces dissipative losses that have a large impact on the accelerator performance.

Indeed, in the first ≥GV/m DWA experiments, beyond quantifying the breakdown thresholds of the dielectric materials, it was also observed that the reflective metal cladding was severely compromised or even destroyed, due to ablation caused by localized heating from the surface currents associated with such large fields [2]. The compromising of the reflective boundary and, the electric dissipation itself, place serious limitations on the use of the DWA as both an ultra-high gradient accelerator and as a narrow-band THz source. An alternate approach with the potential to alleviate such challenges, which provides modal confinement within the DWA structure without the use of external metallic boundaries, is the introduction of photonic structures. Photonic structures are increasingly discussed in a variety of contexts in accelerator design, from radio frequency metallic structures [7], to laser acceleration in dielectric structures [8, 9]. Photonic structures provide flexibility for three-dimensional control over mode characteristics, and may permit damping of undesired higher order modes [7, 10, 11].

Perhaps the most straightforward example of a photonic dielectric accelerator structure is a one-dimensional DWA, with either cylindrical [12] or Cartesian (planar or slab) symmetry, that utilizes Bragg reflectors for confinement. At their essence, Bragg-reflectors are crystalline arrangements consisting of periodic (in 1-D), alternating layers of different dielectric materials which serve to enhance constructive interference of specific wavelengths. Short-wavelength accelerator slab-symmetric geometries (e.g. DWA, or laser-driven structures), are of immediate and compelling interest, when employed in tandem with transversely highly asymmetric (sheet) beams. The confined modes can dramatically diminish coupling to unfavorable transverse wakefields that can lead to beam breakup instabilities [13], and store higher energy, due to the existence of a very wide dimension (taken as x in Fig. 1), thus limiting longitudinal wakefield effects such as beam loading. Indeed, DWA structures with 1-D photonic lattice boundaries (i.e. Bragg-reflectors) can store higher energy for a given gradient in comparison to a

metal boundary confined mode, due to the accumulation of field energy in the reflector itself (see simulation result below in Fig. 4 for illustration of this effect). Such planar structures, in addition to high gradient DWA and laser acceleration applications, may find immediate use in electron beam phase space manipulations, such as beam dechirping for free-electron lasers, where it is necessary to remove the residual chirp imparted on the beam from the compression process [14, 15].

With this background as motivation, in this Letter, we describe the characterization of the electromagnetic response of a THz-scale, 1D photonically confined, slab-symmetric DWA structure based on Bragg-reflectors, that is driven by a high-brightness, relativistic electron-beam. This first experimental test of photonic confinement in a THz DWA was performed at the Brookhaven National Laboratory Accelerator Test Facility (BNL ATF). The fundamental beam-driven mode, dictated in major part by the structure dimensions, is characterized by analyzing the frequency spectrum of the collected coherent Cherenkov radiation as the beam traverses through the vacuum gap of the structure. Simulations results, in both 2D and 3D, as well as an approximate analytical formalism, faithfully reproduce the experimental findings, and provide further insight into the electron beam-wakefield interactions.

The Bragg DWA structure consists of a so-termed matching layer (that dictates the mode frequency, and thus must be matched to the Bragg-reflector used) located nearest to the beam, surrounded by alternating layers of two different dielectric materials (Fig. 1). The matching layer for the structure described here is composed of silicon-dioxide (SiO_2), with permittivity ϵ=3.85 and thickness, d_m=180±5μm. The fundamental mode frequency, f, supported by the structure is a function of both the matching layer thickness and beam gap, and is found by solving the transcendental equation [13],

$$\cot\left[\frac{2\pi f}{c}\sqrt{\epsilon_m-1}(b-a)\right]=\frac{2\pi f}{c}\frac{\sqrt{\epsilon_m-1}}{\epsilon_m}a, \quad (1)$$

where $b=d_m+a$, and c is the speed of light in vacuum. The design fundamental wavelength as determined by the size of the beam gap ($2a$=240μm) and the thickness of the dielectric matching layer given by Eq. 1 is λ =1.435 mm (f =210 GHz).

The design considerations when constructing Bragg-reflectors for a sub-mm DWA structure must include the frequency response of the dielectric materials that compose the reflectors in the THz regime. The reflected components of each alternating dielectric layer interfere constructively, with the strongest interference occurring when the thickness of each layer, d_i, is a quarter wavelength of propagation in that material, at the Cherenkov angle θ_c,

$$d_i=\frac{\lambda}{4n_i\sin\theta_{c,i}}=\frac{\lambda}{4\sqrt{\epsilon_i-1}}, \quad (2)$$

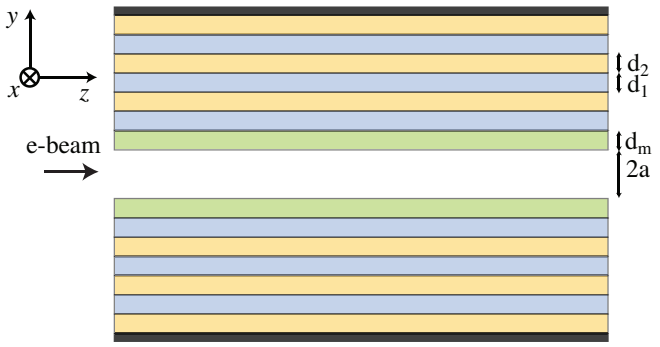

FIG. 1: Sketch of the DWA structure with Bragg-reflector boundaries. The thickness of the matching layer is d_m, and alternating dielectric layers have thickness of d_1 and d_2 respectively. The total beam gap is $2a$.

where $n_i \simeq 1/\sqrt{\epsilon_i}$ is the index of refraction of the material with electric permittivity ϵ_i and the Cherenkov angle is given by, $\cos\theta_{c,i}=1/n_i \simeq 1/\sqrt{\epsilon_i}$. The wavelength of interest, λ, is solely given by the parameters of the initial matching layer (d_m, ϵ_m) and is identical to the case where metallic walls are used as boundaries in place of the Bragg reflector [12]; the Bragg reflection condition reproduces, after a transient, the same response as a conducting boundary. As such, in the 1D limit (ignoring wave variations in the x-direction), the thickness of each subsequent layer, d_i, is determined by the quarter-wavelength condition for constructive interference of Eq. 2.

In order to have an efficient Bragg reflection system, the contrast between the relative permittivities ϵ should be high, to induce large a impedance mismatch at Bragg strata boundaries. Thus the first component of each Bragg period has been chosen to be composed of zirconia-toughened-alumina (ZTA, Zr-Al_2O_3) which is a composite ceramic, with permittivity of ϵ =10.6, which has a low loss tangent in the frequency range of interest (> 75% transmission at f=200GHz) [16], and robust thermal conductivity and capacity. The second component of the Bragg pair is composed of SiO_2. The entire Bragg-reflector stack consists of alternating layers of 115±5μm thick ZTA and 210±5μm thick SiO_2 on either side of the beam gap, totaling 12 periods on each side. The Bragg reflector is assembled by precision layering of the different dielectric slabs (24 mm in x width and 10 mm in z, the beam propagation direction). The beam gap of 240 μm is defined by two short quartz spacers (3 mm x 10 mm) at the transverse ends of the structure (>45 mm away), which also provides structure stability. The complete structure is clamped with aluminum plates for extra support, and mounted on an in-vacuum, remote control 3-axis stage to ensure precision alignment to the electron beam trajectory, as recorded by an alignment laser (<50μm spot size). The experimental layout is similar to that described in detail in Refs. [4, 6].

For these measurements, the BNL ATF delivered an

electron beam of energy $E = 57.6$ MeV, with 0.2% energy spread, normalized emittance $\epsilon_n = 2$ mm-mrad, and charge, Q ∼100 pC. Sextupole correctors ensure that chromatic effects of the beam are corrected through the transport [4, 17]. The beam transverse profile was elliptical, with $\sigma_x = 250\mu$m, and $\sigma_y = 50\mu$m for these measurements. The pulse length of the beam was approximately $\sigma_t \sim 1$ ps selected by masking the beam at a high dispersion point along the transport [18]. The beam bunch profile, and bunch length, is determined using coherent transition radiation (CTR) interferometric techniques coupled with a Kramers-Kronig reconstruction analysis, as in previous BNL ATF studies [19–21].

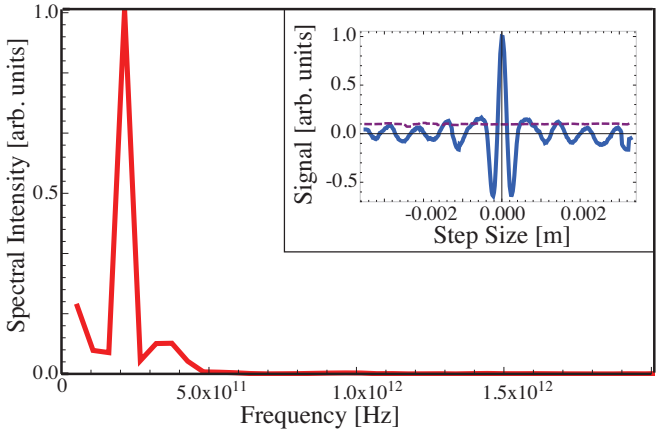

FIG. 2: Fourier transform of the autocorrelation signal, accounting for CTR effects, yields the frequency spectrum of the emitted CCR (red solid). A narrowband spectral peak, centered at ∼210GHz corresponds to the first longitudinal mode of the structure. Inset: Normalized autocorrelation curve (blue solid) of the CCR emission and measured beam charge (purple dashed). The central peak is indicative of beam CTR effects, while the periodic wings are indicative of CCR.

As the beam propagates through the Bragg DWA structure it emits coherent Cherenkov radiation (CCR) at THz frequencies, which propagates to the downstream end of the structure. The DWA assembly incorporates a metallic, rectangular impedance-matched horn antenna with opening angle of 12° to optimally extract the radiation out of the structure into free space. The radiation is collected and collimated using a gold flat and an off-axis paraboloid mirror, respectively, and transported to the interferometer for spectral characterization. The resultant autocorrelation curve is shown in the inset of Figure 2. In the figure, the central peak is indicative of CTR or related coherent diffraction radiation (CDR) signal, due to the electron beam interaction with the longitudinal discontinuities encountered during transport through the structure. The periodic signal found on the wings of the autocorrelation is Fourier transformed to identify the spectral content of the CCR. The beam charge is also monitored, showing stable and consistent running conditions during the course of the interferometric measurements. Fig. 2 shows the result of the frequency analysis of the autocorrelation signal depicting a sharp, narrowband peak at approximately 210 GHz ($\lambda = 1.435$mm) corresponding to the fundamental mode of the Bragg DWA structure in agreement with the design value. The width of this peak is limited from below by the length of wave train contained in the autocorrelation window, not by the intrinsic width given by the full wave train extent.

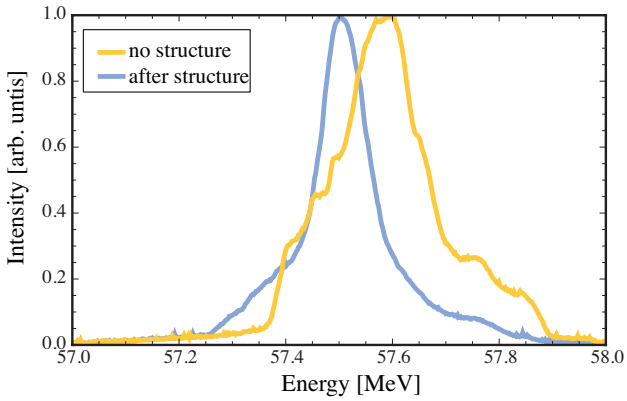

FIG. 3: The normalized measured beam energy profile (yellow) unaffected by the structure shows an energy spread ∼120keV (∼ 0.2%) whereas the beam going through the structure (blue) shows an energy spread ∼60keV (∼ 0.1%) and a mean central energy shift of ∼ 70keV consistent with simulations.

One possibility opened by use the Bragg DWA, is the direct manipulation of the beam longitudinal phase space due to wakefield enabled energy exchange with the structure. In the current case this exchange results in a mitigation of the beam energy chirp [15]. This effect is important in applications of removing residual energy chirp, from the beam compression process, for use in free-electron lasers [14], and has been demonstrated using both dielectric and corrugated metal, slow-wave structures [22, 23]. In the present experiment, the beam energy spectrum is measured using an electromagnet dipole spectrometer and shown in Figure 3. The central energy of the unperturbed beam is $E_0 = 57.6$ MeV with an energy spread of 120 keV (∼ 0.2%). The initial beam has a nearly linear positive chirp (energy at the head higher than at the tail), confirmed by varying the RF linac phase, and simultaneously observing the beam momentum distribution, via optical transition radiation monitors, at a high-dispersion point along the transport. After the beam traverses the Bragg DWA structure, the central energy of the beam shifts by $\Delta E_0 = -70$ keV, with a corresponding beam energy spread of ∼60 keV (∼ 0.1%).

The analytical determination for the magnitude of the peak decelerating field component of the wakefield depends on the beam parameters and structure dimensions, and is given in [13]; a heuristic approximation to these

results, extended to slab-symmetry from the method introduced in [2], is

$$E_{z,dec} = \frac{Q_L}{2\epsilon_0 \left(a + 2\pi\sigma_z \frac{\epsilon_m}{\sqrt{\epsilon_m - 1}}\right)}, \quad (3)$$

where ϵ_0 is the permittivity of free-space, $\sigma_z = c\sigma_t$ is the beam pulse length, and $Q_L = Q/\sqrt{2\pi}\sigma_x$ is the driving beam line charge. For the beam and structure parameters of the experiment, the peak decelerating field is estimated with Eq. 3 to be ∼1.5 MV/m. The field components provided by the heuristic model of Eq. 3 agree with the experimental observed central energy shift and energy spread suppression.

Detailed simulations were used both for experimental design optimization, and for further analysis on the experimental results. Particle-in-cell (PIC) simulation codes used include 2D OOPIC [24] for design work, and 3D Vorpal [25] and CST Microwave Studio [26], for detailed wakefield calculations and beam dynamics studies. Although 2D codes provide valuable insight into the functioning of the Bragg-confined modes, for relevant drive beam shapes 3D codes must be used to understand the experimental results.

The 3D PIC FDTD tracking code, Vorpal, has been shown to generate accurate predictions for wakefields in slab-symmetric beam-driven dielectric structures [27]. Vorpal version 5.2 [25] was used to simulate electron beam excitation of the Bragg DWA structure, including 3D effects. The simulation utilizes a mesh of 1B cells that encompasses the DWA structure with surrounding vacuum regions. The upper and lower dielectric surfaces are treated as perfectly conducting to represent the metallic outer layer in the experiment. The electron beam is represented by a current distribution with Gaussian profiles used to eliminate particle-generated noise. The longitudinal electric field generated in the dielectric gap is ∼1.5 MV/m in amplitude (Fig. 4), consistent with the experimentally measured beam loss and the heuristic model of Eq. 3.

The field evolution through the layers of the Bragg-reflector stack are shown in Fig. 4 (left). A Cherenkov front of appropriate angle in the media is observed, with high frequency components of the wake not confined. On the other hand, the fundamental mode is extremely well confined, as evidenced by the steep drop off of the field from the third period on, reaching nearly zero at the metal boundary. One can see that, as noted above, significant field energy is stored inside the Bragg stack. It is also noteworthy that the wakefield shows strong diffraction effects in the x-z plane (Fig. 4 - middle) in the 3D model [13]. This effect is important for extension of the Bragg geometry to fully-3D lattice symmetries, where total control of diffractive effects is desired.

In addition, one must ask whether excited wakefield mode frequencies are affected by diffraction. In order to examine this question, we utilized the CST simulations, where the bandwidth may be artificially narrowed due to the use of a continuous driving current to excite the structure. The generated frequency is 211±12 GHz, consistent with experimental measurements, as summarized in Figure 5, and with the 2D model that excludes diffractive effects. This mode displays high spectral purity that is ideal for use in narrowband THz applications. Transverse fields are also an important consideration, but as designed, no beam momentum kicks due to transverse wakefields was observed in the experimental data.

In conclusion, we have performed the initial explorations of a simple photonically confined DWA, establishing the expected coupling of an elliptical beam to the slab-symmetric structure, and deducing the characteristics of the excited THz modes. These results, which show mode confinement without the problems of dissipation and structure survivability associated with metals, have direct and immediate application in developing techniques for advanced acceleration and beam manipulation. This important step in DWA photonic structure development was notably performed in the context of elliptical beams, which permit high charge beam acceleration in short wavelength devices. The concepts, modeling, and fabrication techniques developed for this study pave the road for advanced beam and laser-driven, 3D-photonic mode structures with more sophisticated designs. Such experiments, aimed at understanding further mode control in 3D through photonic methods, have been initiated at sub-mm wavelengths. The effects of the Lorentz force associated with transverse wakefields are important in the context of beam break up and emittance dilution [28], and, the Bragg-DWA structure allows for a controlled mitigation of these effects. Finally, beyond wakefield acceleration and phase space manipulation, this type of DWA is well-suited for cross-disciplinary applications, such as a unique, high power, narrowband source of THz radiation. The fact that this is an electron-beam-based source points the way to, for example, utilization of synchronized pump THz pulses as beam-based x-ray FEL radiation probes to enable high-precision, novel experiments in material dynamics.

This work supported by U.S. Dept. of Energy under Contracts No. DE-FG02-07ER46272, No. DE-FG03-92ER40693 and No. DE-AC02-98CH10886, and DARPA under Contract No. N66001-11-1-4197. We gratefully acknowledge the ongoing efforts of the Vorpal development team. This research used resources of the National Energy Research Scientific Computing Center, which is supported by the Office of Science of the U.S. Department of Energy under Contract No. DE-AC02-05CH11231. Author DLB received partial support from the University of Colorado Boulder and from RadiaSoft LLC.

* gerard@physics.ucla.edu

[1] W. Gai, P. Schoessow, B. Cole, R. Konecny, J. Norem, J. Rosenzweig, and J. Simpson, Phys. Rev. Lett. **61**, 2756 (1988).

[2] M. Thompson, H. Badakov, A. Cook, J. Rosenzweig, R. Tikhoplav, G. Travish, I. Blumenfeld, M. Hogan, R. Ischebeck, N. Kirby, et al., Phys. Rev. Lett. **100**, 214801 (2008).

[3] A. M. Cook, R. Tikhoplav, S. Y. Tochitsky, G. Travish, O. B. Williams, and J. B. Rosenzweig, Phys. Rev. Lett. **103**, 095003 (2009).

[4] G. Andonian, O. Williams, X. Wei, P. Niknejadi, E. Hemsing, J. B. Rosenzweig, P. Muggli, M. Babzien, M. Fedurin, K. Kusche, et al., Appl. Phys. Lett. **98**, 202901 (2011).

[5] S. Antipov, C. Jing, A. Kanareykin, J. E. Butler, V. Yakimenko, M. Fedurin, K. Kusche, and W. Gai, Appl. Phys. Lett. **100**, 132910 (2012).

[6] G. Andonian, D. Stratakis, M. Babzien, S. Barber, M. Fedurin, E. Hemsing, K. Kusche, B. O'Shea, X. Wei, O. Williams, et al., Phys. Rev. Lett. **108**, 244801 (2012).

[7] E. I. Smirnova, A. S. Kesar, I. Mastovsky, M. A. Shapiro, and R. J. Temkin, Phys. Rev. Lett. **95**, 074801 (2005).

[8] E. A. Peralta, K. Soong, R. J. England, E. R. Colby, Z. Wu, B. Montazeri, C. McGuinness, J. McNeur, K. J. Leedle, D. Walz, et al., Nature **503**, 91 (2014).

[9] B. Naranjo, A. Valloni, S. Putterman, and J. Rosenzweig, Phys. Rev. Lett. **109**, 164803 (2012).

[10] B. Cowan, Phys. Rev. ST - Accel. and Beams **11**, 011301 (2008).

[11] C. Jing, F. Gao, S. Antipov, Z. Yusof, M. Conde, J. G. Power, P. Xu, S. Zheng, H. Chen, C. Tang, et al., Phys. Rev. ST - Accel. and Beams **12**, 121302 (2009).

[12] A. Mizrahi and L. Schachter, Phys. Rev. E **70**, 016505 (2004).

[13] A. Tremaine, J. Rosenzweig, and P. Schoessow, Phys. Rev. E **56**, 7204 (1997).

[14] K. L. F. Bane and G. Stupakov, Nucl. Instrum. Meth. A **690**, 106 (2012).

[15] S. Antipov, C. Jing, M. Fedurin, W. Gai, A. Kanareykin, K. Kusche, P. Schoessow, V. Yakimenko, and A. Zholents, Phys. Rev. Lett. **108** (2012).

[16] Y. Miyamoto, W. Chen, and S. Kirihara, Transactions of JWRI **36**, 57 (2008).

[17] R. J. England, J. B. Rosenzweig, G. Andonian, P. Musumeci, G. Travish, and R. Yoder, Phys. Rev. ST Accel. Beams **8**, 012801 (2005).

[18] P. Muggli, B. Allen, V. E. Yakimenko, J. Park, M. Babzien, K. P. Kusche, and W. D. Kimura, Phys. Rev. ST Accel. Beams **13**, 052803 (2010).

[19] A. Murokh, J. Rosenzweig, M. Hogan, H. Suk, G. Travish, and U. Happek, Nucl. Instrum. Meth. A **410**, 452 (1998).

[20] R. Lai and A. Sievers, Phys. Rev. E **50**, R3342 (1994).

[21] G. Andonian, A. Cook, M. Dunning, E. Hemsing, G. Marcus, A. Murokh, S. Reiche, D. Schiller, J. B. Rosenzweig, M. Babzien, et al., Phys. Rev. ST - Accel. and Beams **12**, 6 (2009).

[22] P. Emma, M. Venturini, K. L. F. Bane, G. Stupakov, H. S. Kang, M. S. Chae, J. Hong, C. K. Min, H. Yang, T. Ha, et al., Phys. Rev. Lett. **112**, 034801 (2014).

[23] M. Harrison, G. Andonian, T. Campese, A. Murokh, F. H. O'Shea, M. Ruelas, P. Frigola, and M. Fedurin, Proc. of NaPAC13 p. 293 (2013).

[24] D. Bruhwiler and et al., Phys. Rev. ST Accel. Beams **4**, 101302 (2001).

[25] C. Nieter and J. Cary, J. Comput. Phys. **196**, 448 (2004).

[26] http://www.cst.com (2013).

[27] D. Mihalcea, P. Piot, and P. Stoltz, Phys. Rev. ST - Accel. and Beams **15**, 081304 (2012).

[28] A. Chao, R. Richter, and C. Yao, Nucl. Instrum. and Methods A **178**, 1 (1980).

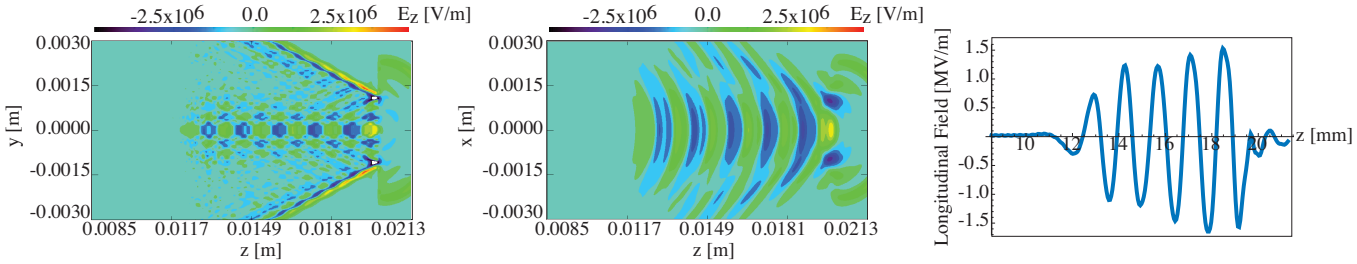

FIG. 4: Simulated longitudinal field contour plot using experimental parameters from Vorpal shows a peak field of ∼1.5 MV/m, dispalyed as a function of vertical coordinate (bisecting Bragg layers) - left, and horizontal coordinate (parallel to Bragg layers) - middle. The longitudinal projection of E_z on-axis is shown on the right. The electron beam travels in the positive-z direction.

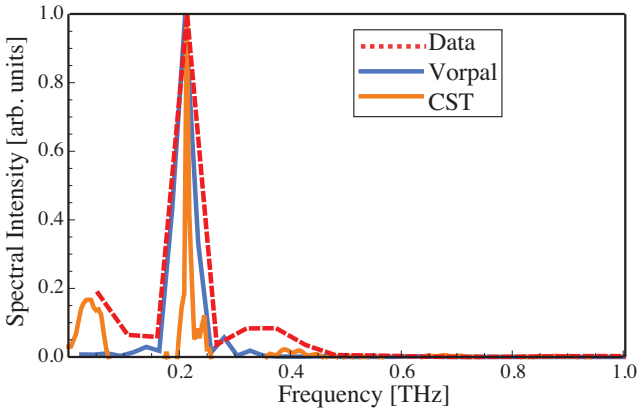

FIG. 5: Comparison of simulation results with data (dashed red). Vorpal (blue) and CST (orange) yield the same resonant mode for the Bragg DWA structure.